CHINESE OPTICS LETTERS

Vol. 20, No. 12 | December 2022

Multifunctional single-fiber optical tweezers for particle trapping and transport

Hao Wu (吴 昊)[1], Chunlei Jiang (姜春雷)[1*], Shaopeng Tian (田绍鹏)[2], Shangzhao Shao (邵上钊)[1], Hangyu Yue (岳航宇)[1], Xiangyu Cui (崔翔宇)[1], Bingkun Gao (高丙坤)[1], Xiufang Wang (王秀芳)[1], and Peng Chen (陈 朋)[1]

[1] College of Electrical and Information Engineering, Northeast Petroleum University, Daqing 163318, China

[2] The Third Oil Production Plant of Daqing Oilfield Co., Daqing 163113, China

*Corresponding author: jiangchunlei_nepu@163.com

Received February 4, 2022 | Accepted June 17, 2022 | Posted Online September 22, 2022

We present and demonstrate a multifunctional single-fiber optical tweezer for particle trapping and transport. The fiber probe of fiber optical tweezers is constructed as a planar structure. Laser sources with wavelengths of 650 nm and 980 nm in a single-mode fiber excite the linearly polarized LP_{11} mode and LP_{01} mode beams, respectively. These two laser beams can achieve non-contact trapping and long-distance transport of particles after passing through a flat-facet fiber probe, respectively. This structure makes it possible to perform non-contact trapping and transport of particles by combining multiple wavelengths and multiple modes.

Keywords: fiber optical tweezers; particles; optical trapping; optical transportation.
DOI: 10.3788/COL202220.121201

1. Introduction

The trapping and targeted transport of particles has been rapidly developed due to its great value for applications in biomedical, physical, and chemical fields[1–5]. Different strategies have been proposed for particle trapping and transport, such as optical forces, magnetic fields, dielectrophoresis, and mechanical forces. Optofluidic devices based on planar optical waveguides have the advantages of compact structure, easy access to experimental samples, etc., and can trap and transport particles[6]. The organization and transport of particles can be performed by embedding magnetrons[7], electrodes[8], and mechanical components[9] into the microfluidic device. Since fiber optical tweezers can trap particles in a very narrow space, they also have a great advantage for particle trapping and transport. Many types of fiber optical tweezers have been developed, such as multi-fiber optical tweezers[10], single-fiber optical tweezers[11–13], and near-field optical tweezers[14–16].

In recent years, some fiber optical tweezers obtained by combining other cutting-edge technologies, models, and materials have also been developed, for example, single-fiber microstructure optical tweezers[17–19], opto-thermophoretic tweezers[20], and coating graphene[21] on the exit end of the optical fiber. These fiber optical tweezers can achieve particle trapping, positioning, and even rotation[22] operations. Simultaneous trapping of two particles can also be achieved by using a single-wavelength laser source to excite different mode beams[23]. With the rapid development of the field of micromanipulation, more and more functions have been demanded from fiber optical tweezers. Therefore, it is necessary to use fiber optical tweezers to achieve more operational functions and improve their utilization efficiency and integration. Currently, the implementation of particle trapping and transport is of great significance in applications such as targeted drug delivery. Because of the simple and effective structure of fiber optical tweezers, it is necessary to use it to achieve both particle trapping and transport of particles. Several methods of particle trapping and transport using fiber optical tweezers have emerged. In 2012, Li *et al.* realized the trapping and transport of particles on the fiber surface by using the evanescent field generated on the surface of the submicron fiber[15]. In 2015, Cao *et al.* used a laser source of one wavelength to excite different modes and then used a mode selector to convert the different modes to achieve particle trapping and transport[24,25]. In 2015, Zhang *et al.* used the thermophoretic force generated by the thermal effect for the emission of trapped particles[26]. In 2016, Zeltner *et al.* used a hollow-core photonic crystal fiber to achieve particle trapping and guidance inside the fiber[27]. In 2017, Yuan *et al.* implemented a fiber gun for 10 μm size particle emission using a homemade coaxial core fiber[28]. However, none of the above methods involve the use of multiple wavelengths in combination with multi-mode beams for non-contact trapping and transport of particles.

Therefore, in this paper, we propose and demonstrate an all-fiber device that enables particle trapping and transport on the basis of a common single-mode fiber. First, laser sources with

wavelengths of 650 nm and 980 nm are injected into a single-mode fiber with a typical operating wavelength of 980 nm, respectively. Then, the linearly polarized LP_{11} and LP_{01} mode beams are excited separately in the single-mode fiber. By making the fiber tip into a special flat-facet shape, the trapping force and scattering force can be generated by the LP_{11} mode beam and LP_{01} mode beam, respectively. This structure allows not only the non-contact trapping of particles but also the transport of particles without moving the fiber. In addition, we have established a simulation model by finite element analysis method, and the simulation results support our experimental results.

2. Principle and Numerical Simulation

Fiber probes are fabricated using commercial single-mode fibers (Model: CS980-125-16/250, core diameter: 4.7 μm, cladding diameter: 125 μm; YOFC) by flame heating techniques[29]. The buffer layer and polymer jacket of the fibers are first stripped by using a fiber stripper. The stripped length of the fiber is 5 cm. To prevent it from breaking and warping, the fibers are wrapped with stainless steel capillaries (outer diameter: 0.5 mm, wall thickness: 0.1 mm, length: 100 mm). The fiber is heated for about 30 s to reach the melting point and then drawn at an initial speed of about 1.5 mm/s. The fiber diameter was reduced from 125 μm to 19.5 μm over a length of 5.27 mm. Then, it was sped up and drawn at a speed of about 16 mm/s. The fiber broke into a plane with a diameter of 8.1 μm. Finally, the fiber probe is completed by gently wiping the fiber tip with an alcohol-impregnated cotton towel.

Microcavities are made by heating and drawing glass capillaries and then placing microspheres in them. First, they are sealed by heating the ends of the glass capillary tubes (inner diameter: 0.1 mm, wall thickness: 0.1 mm, length: 100 mm). Then, heating was applied for about 12 s, followed by drawing at a rate of about 1.2 mm/s. The capillary diameter was reduced from 0.3 mm to 6.7 μm over a length of 7.86 mm. At this time, the heating and stretching of the capillary are stopped. The capillary is stretched at a speed of about 10 mm/s after the capillary has cooled for about 5 s. The end face of the capillary tube forms a hollow-core microtubule with an outer diameter of 6.7 μm and an inner diameter of 4.2 μm. Finally, polystyrene microspheres with a diameter of 6 μm are placed in the capillary to complete the microcavity.

The experimental setup is shown in Fig. 1(a). We realize the coupling of the 980 nm and 650 nm laser sources by using a 2×1 fiber coupler. The output end of the fiber coupler is first connected to a section of G652D single-mode fiber and then spliced with a single-mode fiber at a typical working wavelength of 980 nm using a fiber fusion splicer. The 980 nm laser source excites the LP_{01} mode beam in a single-mode fiber at a typical operating wavelength of 980 nm. The 650 nm laser source excites the LP_{11} mode beam in a single-mode fiber. The beams of different modes generated by the two wavelengths achieve different degrees of focusing through a specially designed flat-facet fiber probe. Then, the trapping and transportation of particles

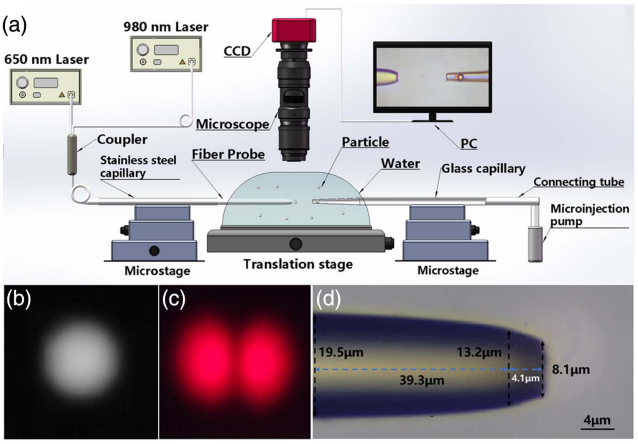

Fig. 1. (a) Schematic of the experimental setup. (b) Image of far-field light intensity distribution of the excited LP_{01} mode beam. (c) Image of far-field light intensity distribution of the excited LP_{11} mode beam. (d) Optical micrographic image of flat-facet fiber probe.

using this structure are realized. The fiber probe is fixed on the precision five-axis microstage to achieve precise positioning. The fiber probe is wrapped with a stainless steel capillary tube to prevent it from breaking and bending. The fiber probe is immersed in the microsphere suspension, and the microsphere suspension is dropped on a glass slide installed on a three-axis translation stage. The image is collected by a CCD and observed in real time on the computer. The glass capillary is connected to an external microinjection pump via a connecting tube to maintain pressure balance. To facilitate observation, a filter that filters out 97% of the 650 nm scattered light is placed in the CCD.

The normalized frequency V is an important parameter for determining the transmission mode in a fiber. The LP_{01} mode beam is excited in the fiber when $V < 2.405$. The LP_{11} mode beam is excited in the fiber when $2.405 \leq V \leq 3.832$. Other higher-order modes can be excited in the fiber when $V > 3.832$. When a laser beam with a wavelength of 980 nm is injected into a single-mode fiber with a typical operating wavelength of 980 nm, $V = 2.223 < 2.405$, and the LP_{01} mode beam is excited in the single-mode fiber. The far-field light intensity distribution of the LP_{01} mode beam is shown in Fig. 1(b). When a laser beam with a wavelength of 650 nm is injected into a single-mode fiber with a typical operating wavelength of 980 nm, $2.405 < V = 3.352 < 3.832$, the LP_{11} mode beam is excited in the single-mode fiber. The far-field light intensity distribution of the LP_{11} mode beam is shown in Fig. 1(c). Water exhibits low absorption for both wavelengths of laser light. Therefore, no temperature gradients are generated to cause turbulence, which ensures stable manipulation. The difference between ordinary tapered single-fiber optical tweezers in trapping particles is not obvious when using the LP_{01} mode or LP_{11} mode for trapping particles. The experimental results are shown in Fig. 2. Therefore, we fabricated a flat-facet fiber probe. The LP_{11} mode beam forms an effective optical trap for particle trapping after passing through the flat-facet fiber probe. The

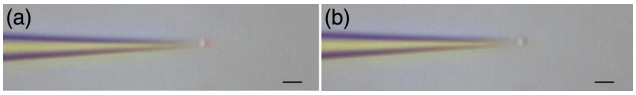

Fig. 2. Tapered fiber probe traps particles in the experiment. (a) Particle trapping was performed using an LP_{11} mode beam excited by a 650 nm laser source. (b) Particle trapping was performed using an LP_{01} mode beam excited by a 980 nm laser source. (The scale bars in the figure are all 4 μm.)

LP_{01} mode beam always exhibits a scattering force capable of pushing particles away from the fiber tip after passing through the flat-facet fiber probe and is used for particle transport. The microscopic image of the fiber probe is shown in Fig. 1(d).

We established a simulation model through finite element analysis. The total light force F_0 exerted on the particle can be expressed as follows[30]:

$$F_0 = \oint_S (\langle T_M \rangle \cdot n) \mathrm{d}S, \tag{1}$$

where the integration is taken over a closed surface S surrounding the particle, n is the surface normal vector, and T_M is the time-independent Maxwell stress tensor, which can be calculated as follows:

$$T_M = \frac{1}{2}\mathrm{Re}\left[\varepsilon EE^* + \mu HH^* - \frac{1}{2}(\varepsilon|E|^2 + \mu|H|^2)I\right], \tag{2}$$

where EE^* and HH^* indicate the outer product of the electromagnetic fields; ε is the electric permittivity; μ is the magnetic permeability; I denotes the unit dyadic.

We use the wave optics module (electromagnetic waves, frequency domain) and perfectly matched layer boundary conditions to perform simulations in commercial finite element simulation software. The refractive indices of fiber, particle, and water are set to 1.45, 1.45, and 1.33, respectively. The particle diameter is set to 2 μm. The wavelengths are set to 650 nm and 980 nm, respectively. The input power is set to 1 W/m. The LP_{11} mode beam [Figs. 1(c), 3(a), and 3(b)] has almost no power distribution in the x axis. Its power is mainly concentrated on the sides of the beam[31]. The LP_{11} mode beam has a trapping point in the x axis at a distance of 3.7 μm from the fiber probe. The force applied on the particles is positive before 3.7 μm, pushing the particles towards the trapping point. The force on the particles is negative in the range of 3.7 μm to 7.3 μm, pulling the particles back to the trapping point. After 7.3 μm, the force applied on the particle becomes positive again, pushing the particle away from the fiber optic probe. The electric field distribution, details of the electric field distribution, and force analysis are shown in Figs. 3(a)–3(c), respectively. The force analysis of the particle was performed at 3.7 μm and 10 μm in the y-axis direction, respectively. The simulation results show that if the particle deviates from the x axis, it is pulled back to the x axis by a force that is opposite its direction of motion. The force analysis is shown in Fig. 3(d). Thus, the particle can remain in the axis while being trapped or while being transported.

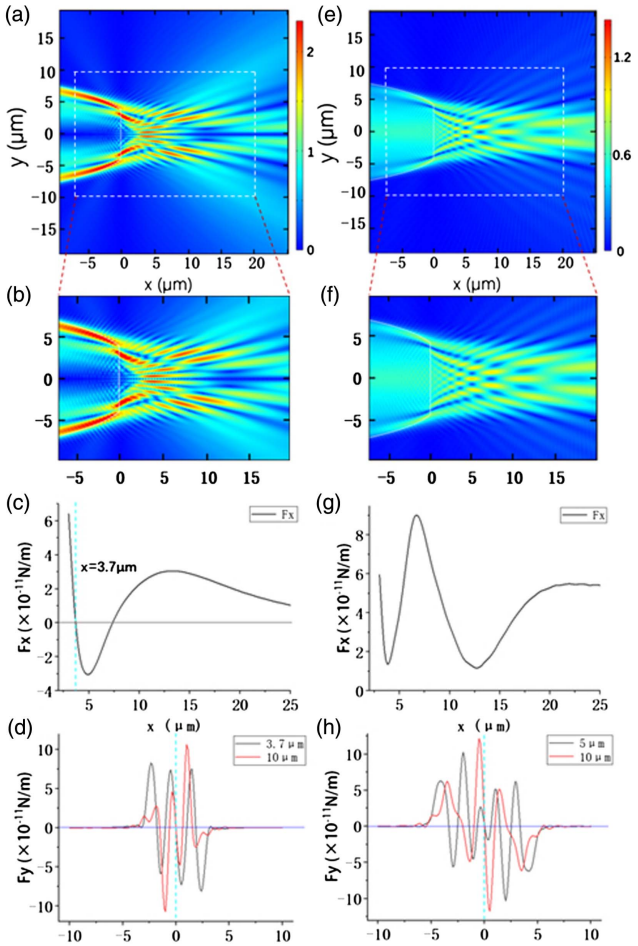

Fig. 3. (a)–(d) LP_{11} mode beam excited by a 650 nm laser passes through the electric field of the flat-facet fiber probe, details of the electric field distribution, applying a force on the particle in the x axis and a force on the particle along the y-axis direction. (e)–(h) LP_{01} mode beam excited by a 980 nm laser passes through the electric field of the flat-facet fiber probe, details of the electric field distribution, applying a force on the particle in the x axis and a force on the particle along the y-axis direction.

The power of the LP_{01} mode beam [Figs. 1(b), 3(e) and 3(f)] is mainly concentrated in the middle of the beam[29]. It does not achieve strong focus to form an optical trap after passing through the fiber probe. The force it exerts on the particle in the x axis is always expressed as a scattering force that pushes the particle away from the fiber probe. The force on the particle is always positive. The electric field distribution, details of the electric field distribution, and force analysis are shown in Figs. 3(e)–3(g), respectively. The force analysis was performed at 5 μm and 10 μm in the y-axis direction, respectively. The simulation results show that if the particle deviates from the x axis, it is pulled back to the x axis by a force that is opposite its direction of motion. Thus, the particle can be kept in the axis all the time while being transported. The force analysis is shown in Fig. 3(h). Therefore, we construct a non-contact trapping point, as can be seen from the above force analysis. Moreover, the particles can be transported along the x axis outside the trapping point.

3. Experimental Results and Discussions

Only the laser source with a wavelength of 650 nm was turned on, and the fiber probe output power was 5.33 mW. Silica particles with a diameter of 2 μm achieve non-contact trapping at a distance of about 2.7 μm from the fiber tip. By manipulating the fiber optic probe, the trapped particles can move about 42.36 μm along the $+x$ direction [Fig. 4(b)]. Continuing to manipulate the fiber probe, the trapped particles could move about 47 μm [Fig. 4(c)], 28.9 μm [Fig. 4(d)], and 41.18 μm [Figs. 4(e) and 4(f)] along the $-x$, $-y$, and $+y$ directions, respectively. In addition, the trapped particles can be released when the laser source is turned off. This indicates that the dynamic operation is caused by the movement of the fiber probe.

When $t = 0$ s, the particles are in the state of trapping using a 650 nm laser source. Turning on the 980 nm laser source, the output power at the fiber probe end is 4.03 mW. At this point, the push force exerted on the particle by the 980 nm laser source is greater than the trapping force exerted on the particle by the 650 nm laser source, so the particle breaks away from the optical trap for emission. The distances of the particles from the fiber tip at $t = 4$ s, 11 s, 17 s, and 23 s are 8.3 μm, 42.6 μm, 73.3 μm, and 91.6 μm, respectively. The partial trajectory images and detailed position information of the particle motion are shown in Figs. 5(a) and 5(b). The thrust force applied to the particle gradually decreases as it gets farther and farther from the fiber tip. Finally, the longest emission distance of the particle is 122.3 μm.

The particles will not achieve trapping, only emission, when only the 980 nm laser source is turned on. When $t = 0$ s, the particle is moved to the front of the fiber probe, and it is emitted along the axial direction. The distances of particles from the fiber probe tip at $t = 2$ s, 20 s, 30 s, and 42 s are 8.6 μm, 32.3 μm, 60.2 μm, and 86 μm, respectively. The maximum emission distance of the particles is 86 μm. The partial trajectory images and detailed position information of the particles during the emission are shown in Figs. 6(a) and 6(b), respectively. The emission distance of particles is reduced by 36.3 μm compared to two laser sources turned on simultaneously. In addition, the average velocity is reduced from 4.13 μm/s to 2.05 μm/s when emitted to 86 μm. Compared to two laser sources turned on at the same

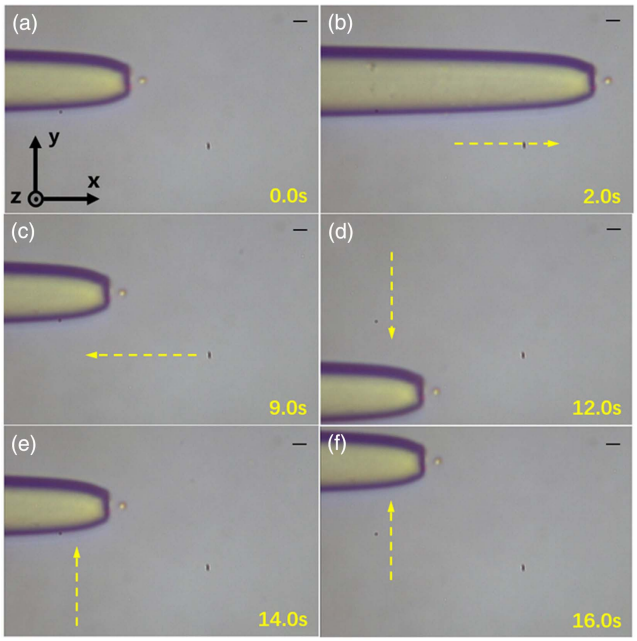

Fig. 4. Manipulation of particles in the x–y plane. (The scale bars in the figure are all 4 μm.)

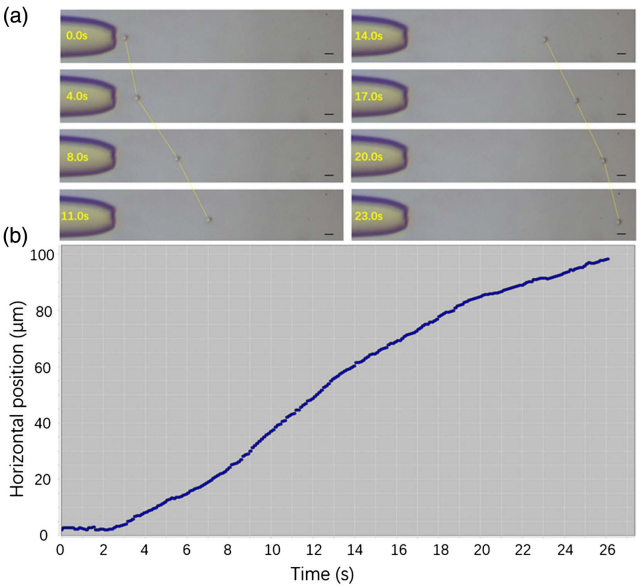

Fig. 5. (a) Trajectory of particles being emitted when the 650 nm and 980 nm laser sources are turned on simultaneously. (The scale bars in the figure are all 4 μm.) (b) The horizontal position of the particle as a function of time.

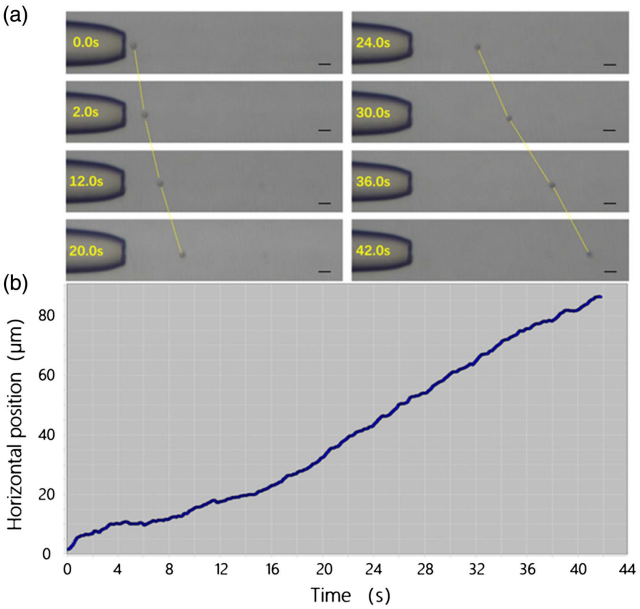

Fig. 6. (a) Particle emission trajectory when only the 980 nm laser source is turned on. (The scale bars in the figure are all 4 μm.) (b) The horizontal position of the particle as a function of time.

time, the combined force of the thrust applied to the particles in the axial direction is reduced when only the 980 nm laser source is used for particle emission. So, the emission distance and emission velocity of particles are reduced. Therefore, we can achieve not only the non-contact trapping of particles, but also the emission of particles over longer distances and at faster speeds when two laser sources are used.

Based on the fact that we can achieve not only particle manipulation but also particle emission, we achieve particle transport. We show two of the processes of particle transport. The first transport process is shown in Fig. 7 (the microcavity is at the position of 35.6 μm in the $-y$ direction and 74.1 μm in the $+x$ direction of the particle). First, we use a 650 nm laser source to achieve non-contact trapping of particles and then move the fiber probe 40.2 μm in the $-y$ direction [Figs. 7(a) to 7(b)]. The 980 nm laser source is turned on, and the particles start to be transported. The distances between the particle and the fiber probe at 12 s and 21 s are 23 μm [Fig. 7(c)] and 72.8 μm [Fig. 7(e)], respectively. At 25 s, the particles are transported to the microcavity at a distance of 78.8 μm from the fiber probe [Fig. 7(f)]. The final transport distance of the particles is 86.8 μm [Fig. 7(g)].

The second process is shown in Fig. 8 (the microcavity is at the position of 44.3 μm in the $+y$ direction and 45.7 μm in the $+x$ direction of the particle). First, we use a 650 nm laser source to achieve non-contact trapping of particles and then move the fiber probe 48.6 μm in the $+y$ direction [Figs. 8(a) to 8(b)].

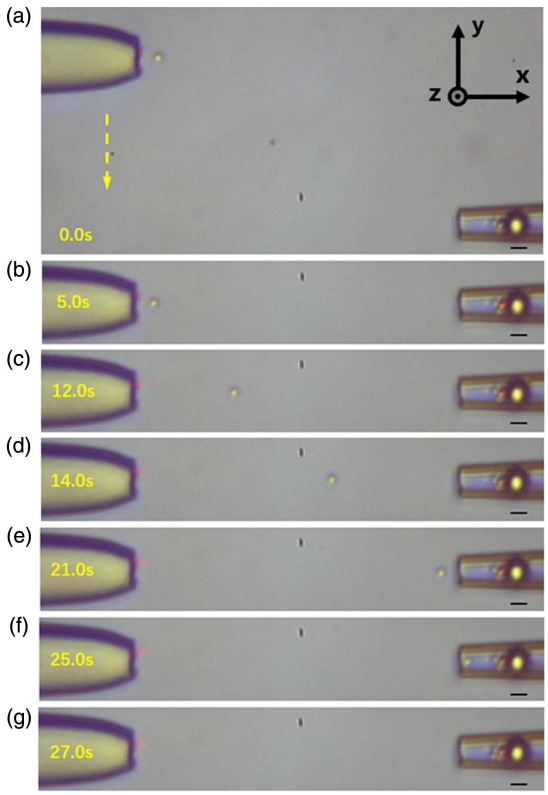

Fig. 7. First transport process of the particle. (The scale bars in the figure are all 4 μm.)

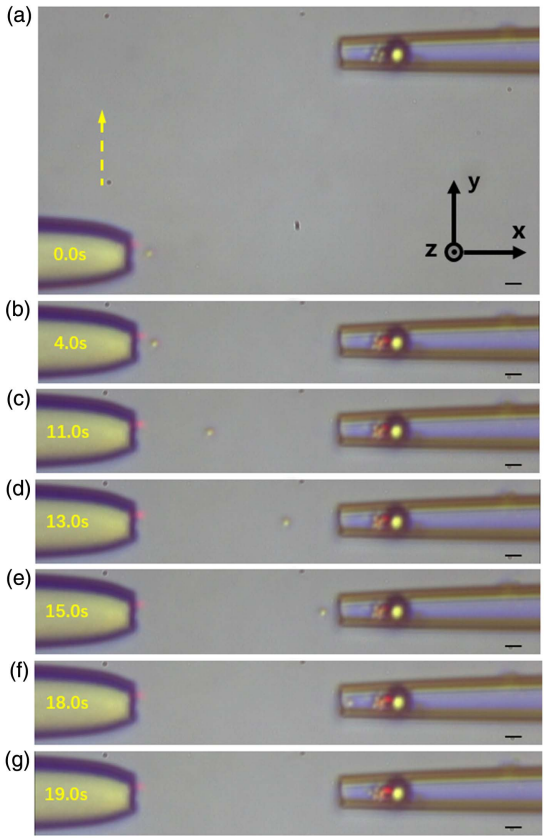

Fig. 8. Second transport process of the particles. (The scale bars in the figure are all 4 μm.)

The 980 nm laser source is turned on, and the particles start to be transported. The distances between the particle and the fiber probe at 11 s and 15 s are 17 μm [Fig. 8(c)] and 44.5 μm [(Fig. 8(e)], respectively. At 18 s, the particles are transported to the microcavity at a distance of 49.8 μm from the fiber probe [Fig. 8(f)]. The final transport distance of the particles is 56.3 μm [Fig. 8(g)].

4. Conclusions

In this paper, we design and demonstrate a multifunctional single-fiber optical tweezer. It enables non-contact trapping and long-distance transport of particles. The structure uses a 650 nm laser source and a 980 nm laser source to generate the LP_{11} mode beam for non-contact particle trapping and the LP_{01} mode beam for particle transport, respectively. So, the different laser wavelengths can excite different modes to achieve different functions in fiber optical tweezers. This method uses a small laser power output, and the laser wavelength used can effectively reduce the photothermal effect during particle manipulation. As a controllable all-fiber integration device, it expands the characteristics of single-fiber optical tweezers and provides the possibility for more practical applications in the field of micromanipulation research. It promotes the development of trapping and transport of particles. It offers

more possibilities for particle sorting, targeted drug delivery, etc., in biology.

Acknowledgement

This work was supported by the Joint Guidance Project of Natural Science Foundation of Heilongjiang Province, China (No. LH2021F008).

References

1. Y. Li and Y. Hu, "Optical trapping and controllable targeted delivery of nanoparticles by a nanofiber ring," Appl. Phys. B **124**, 216 (2018).
2. X. Liu, Y. Wu, X. Xu, Y. Li, Y. Zhang, and B. Li, "Bidirectional transport of nanoparticles and cells with a bio-conveyor belt," Small **15**, 1905209 (2019).
3. J. El-Ali, P. K. Sorger, and K. F. Jensen, "Cells on chips," Nature **442**, 403 (2006).
4. S. Nagrath, L. V. Sequist, S. Maheswaran, D. W. Bell, D. Irimia, L. Ulkus, M. R. Smith, E. L. Kwak, S. Digumarthy, and A. Muzikansky, "Isolation of rare circulating tumour cells in cancer patients by microchip technology," Nature **450**, 1235 (2007).
5. P. S. Dittrich, K. Tachikawa, and A. Manz, "Micro total analysis systems. Latest advancements and trends," Anal. Chem. **78**, 3887 (2006).
6. X. Fan and I. M. White, "Optofluidic microsystems for chemical and biological analysis," Nat. Photonics **5**, 591 (2011).
7. N. Pamme and C. Wilhelm, "Continuous sorting of magnetic cells via on-chip free-flow magnetophoresis," Lab Chip **6**, 974 (2006).
8. P. Puri, V. Kumar, S. U. Belgamwar, and N. N. Sharma, "Microfluidic device for cell trapping with carbon electrodes using dielectrophoresis," Biomed. Microdevices **20**, 102 (2018).
9. T. Jian, P. Rong, and J. Ding, "The regulation of stem cell differentiation by cell-cell contact on micropatterned material surfaces," Biomaterials **31**, 2470 (2009).
10. L. B. Yuan, Z. H. Liu, J. Yang, and C. Y. Guan, "Twin-core fiber optical tweezers," Opt. Express **16**, 4559 (2008).
11. Y. Li, H. Xin, X. Liu, and B. Li, "Non-contact intracellular binding of chloroplasts *in vivo*," Sci. Rep. **5**, 10925 (2015).
12. Z. Liu, C. Guo, J. Yang, and L. Yuan, "Tapered fiber optical tweezers for microscopic particle trapping: fabrication and application," Opt. Express **14**, 12510 (2006).
13. R. Taylor and C. Hnatovsky, "Particle trapping in 3-D using a single fiber probe with an annular light distribution," Opt. Express **11**, 2775 (2003).
14. Y. Zhang, H. Lei, and B. Li, "Refractive-index-based sorting of colloidal particles using a subwavelength optical fiber in a static fluid," APEX **6**, 072001 (2013).
15. H. Lei, C. Xu, Y. Zhang, and B. Li, "Bidirectional optical transportation and controllable positioning of nanoparticles using an optical nanofiber," Nanoscale **4**, 6707 (2012).
16. H. Lei, Y. Zhang, X. Li, and B. Li, "Photophoretic assembly and migration of dielectric particles and Escherichia coli in liquids using a subwavelength diameter optical fiber," Lab Chip **11**, 2241 (2011).
17. Z. Yu, Z. Liu, J. Yang, and L. Yuan, "Four-core optical fiber micro-hand," J. Light. Technol. **30**, 1487 (2012).
18. Y. Zhang, Z. Liu, J. Yang, and L. Yuan, "An annular core single fiber tweezers," Sens. Lett. **10**, 1374 (2012).
19. C. Liberale, P. Minzioni, F. Bragheri, F. D. Angelis, E. D. Fabrizio, and I. Cristiani, "Miniaturized all-fibre probe for three-dimensional optical trapping and manipulation," Nat. Photonics **1**, 723 (2007).
20. A. Kotnala and Y. Zheng, "Opto-thermophoretic fiber tweezers," Nanophotonics **8**, 475 (2019).
21. Z. Li, J. Yang, S. Liu, X. Jiang, H. Wang, X. Hu, S. Xue, S. He, and X. Xing, "High throughput trapping and arrangement of biological cells using self-assembled optical tweezer," Opt. Express **26**, 34665 (2018).
22. B. J. Black and S. K. Mohanty, "Fiber-optic spanner," Opt. Lett. **37**, 5030 (2012).
23. Y. Zhang, Y. Zhou, X. Tang, Z. Wang, Y. Zhang, Z. Liu, J. Zhang, J. Yang, and L. Yuan, "Mode division multiplexing for multiple particles noncontact simultaneous trap," Opt. Lett. **46**, 3017 (2021).
24. E. Zhao, Z. Liu, Y. Zhang, Y. Zhang, J. Yang, and L. Yuan, "A mode-division-multiplexing single fiber optical tweezers," Proc. SPIE **9655**, 96551D (2015).
25. Z. H. Liu, P. B. Liang, Y. Zhang, J. J. Lei, Y. X. Zhang, J. Yang, and L. B. Yuan, "A micro-particle launching apparatus based on mode-division-multiplexing technology," Opt. Commun. **342**, 30 (2015).
26. Z. Liu, P. Liang, Y. Zhang, Y. Zhang, E. Zhao, J. Yang, and L. Yuan, "Micro particle launcher/cleaner based on optical trapping technology," Opt. Express **23**, 8650 (2015).
27. R. Zeltner, D. S. Bykov, S. Xie, T. G. Euser, and P. S. J. Russell, "Fluorescence-based remote irradiation sensor in liquid-filled hollow-core photonic crystal fiber," Appl. Phys. Lett. **108**, 231107 (2016).
28. H. Deng, Y. Zhang, T. Yuan, X. Zhang, Y. Zhang, Z. Liu, and L. Yuan, "Fiber-based optical gun for particle shooting," ACS Photonics **4**, 642 (2017).
29. H. Xin, Q. Liu, and B. Li, "Non-contact fiber-optical trapping of motile bacteria: dynamics observation and energy estimation," Sci. Rep. **4**, 6576 (2014).
30. B. S. Schmidt, A. Yang, D. Erickson, and M. Lipson, "Optofluidic trapping and transport on solid core waveguides within a microfluidic device," Opt. Express **15**, 14322 (2007).
31. Z. Liu, L. Wang, P. Liang, Y. Zhang, J. Yang, and L. Yuan, "Mode division multiplexing technology for single-fiber optical trapping axial-position adjustment," Opt. Lett. **38**, 2617 (2013).